Proceedings World Geothermal Congress 2020+1
Reykjavik, Iceland, April - October 2021

Dynamics of Natural Rock Fractures in the EGS Revealed Via the Pressurized Water Injection Experiments in Laboratory

Takuya Ishibashi, Hiroshi Asanuma, and Noriaki Watanabe

FREA, AIST, 2-2-9, Machiikedai, Koriyama, Fukushima, 963-0298, Japan

Takuya.ishibashi@aist.go.jp

Keywords: Shear slip, Permeability, Fracture propagation, EGS, Fluid injection

ABSTRACT

In order to suggest the optimal design of Enhance Geothermal Systems (EGS), we need to understand the dynamics of pre-existing rock fractures during pressurized water injection into the geothermal reservoirs precisely. Especially, the shear slip on fractures and the fracture propagation from tips/asperity contacts of fractures should be carefully investigated and modelled, since these mechanisms could vary the mechanical and hydraulic properties of geothermal reservoir drastically. Our study presents the experimental results those explore the linkage between strength, strain/slip distance, permeability, and acoustic emissions of the fractured rock of granite during hydraulic shearing/fracturing under high stress condition (e.g., both normal and shear stresses on pre-existing fracture are more than 50 MPa) assuming the geothermal reservoir environment. Through the experiments, we successfully constrain the failure criteria, maximum strain/slip distance, maximum permeability change, and so on for the fractured rock in laboratory-scale. Based on these experimental results, we further discuss how these parameters vary depending on the representative scales of the reservoir. Such information would be indispensable to determine the actual injection protocol in the EGS developments.

1. INTRODUCTION

Hydraulic stimulation on the geothermal reservoir is the well-known operation for improving or maintaining the transmissivity and fracture connectivity within the reservoir (Evans et al., 2005; Häring et al., 2008). In this operation, by injecting pressurized water into the reservoirs, pre-existing fractures are reactivated in shearing mode with the opportunity for self-propping on asperities (Esaki et al., 1999). Due to these mechanisms, mechanical and hydraulic properties of fracture/fracture network evolve. During the shear slip on fractures, seismicity is possibly increased (Ellsworth, 2013; Majer et al., 2007), and it is necessary to be explored how the mechanical-hydraulic properties evolve and link in each other during the hydraulic shearing.

With respect to the mechanical-hydraulic coupling on the single fault during hydraulic shearing, Guglielmi et al. (2015a and 2015b) have reported the experimental results of in-situ reactivation of meso-scale single fault (e.g., both carbonate and shale formations). Their studies successfully reveal the friction, permeability, and microearthquake evolutions and that slow/aseismic slip primarily and initially occurs and then triggers the micro-earthquakes. This finding is possibly useful in assessing the seismic hazard associated with the pressurized water injection into the fractured systems underground. However, when we consider the pre-existing fractures/faults within geothermal reservoirs, it is unclear whether the aforementioned findings are directly applicable to the seismic risk mitigation or not. This is because (i) the mechanical and frictional properties of granite are obviously different from those of carbonate or shale (Ikari et al., 2011; Kohli and Zoback, 2013), and (ii) the crustal stresses are generally several tens of mega-pascals or more, which is much higher values than those assumed in the aforementioned in-situ fault reactivation experiments (e.g., less than ten mega-pascal), in typical geothermal systems (Evans et al., 2005; Häring et al., 2008; Norbeck et al., 2018).

That's why the recent researches have begun to draw attentions on the shear slip/fracture propagation caused by the pressurized water injection under relatively high stress states (Rutter and Hackston, 2017 and Ishibashi et al., 2018). As far as we know, Ye and Ghassemi (2018) have reported the first study, which carefully explores the injection-driven shear slip under the simulated conditions of the geothermal reservoir environment. Via their novel experiments, they successfully demonstrate that the retainable permeability enhancement is achieved due to the dilatant shear slip (so-called "self-propping shear slip concept"). On the other hands, failure criteria, full spectral of hydraulic shearing process, and so on, which are essential for the numerical simulation on the optimal EGS design, are still not revealed, since they haven't varied the stress state and also haven't recorded the acoustic emissions.

With these in minds, our study presents the experimental results those explore the linkage between mechanical and hydraulic properties of the fractured rock of granite during hydraulic shearing/fracturing under high stress condition (e.g., both normal and shear stresses on pre-existing fracture are more than 50 MPa) assuming the geothermal reservoir environment. In our study, we vary the stress states and also record the acoustic emissions during the injection-driven shear slip to explore the failure criteria, full spectral of hydraulic shearing process, and so on. Based on the experimental results, we discuss how we can apply the laboratory experimental results to the field scale (mesoscale) problems. Such discussions would be indispensable to determine the actual injection protocol in the EGS developments.

2. METHODS

In this study, we commonly use the cylindrical sample (50 mm in diameter and 100 mm in length) of Inada medium-grained granite (Ibaraki, Japan) containing a single tensile fracture, which inclines 45degree to the cylindrical axis (Figure 1a). Borehole (1.5 mm in diameter) is set for both sides of separated rock samples, that enables us the fluid injection experiments. Before conducting the pressurized water injection experiments, we measure the surface topographies of the tensile fracture (both footwall and hanging wall) in a 23.433 μm square grid system with the 3D measuring microscope (Keyence, VR-3050). Height resolution of the 3D microscope is reported to be 0.01 μm. Representative result for the fracture surface profiling is shown in Figure 1b. Based on the digital data of

fracture surfaces, we evaluate the roughness parameters of the vertical interval, Sz, and RMS (Root Mean Square). Representative values of Sz and RMS are 6.5mm and 1.5 mm, and they are much larger than those for the fractures roughened by silicon carbide. Figure 1c shows the representative relationship between PSD (Power Spectral Density) and spatial frequency for both foot wall and the hanging wall of the fracture. Fractal dimension for the fracture surfaces are evaluated to be 2.4, and a series of roughness parameters are consistent with our previous study (Ishibashi et al., 2016).

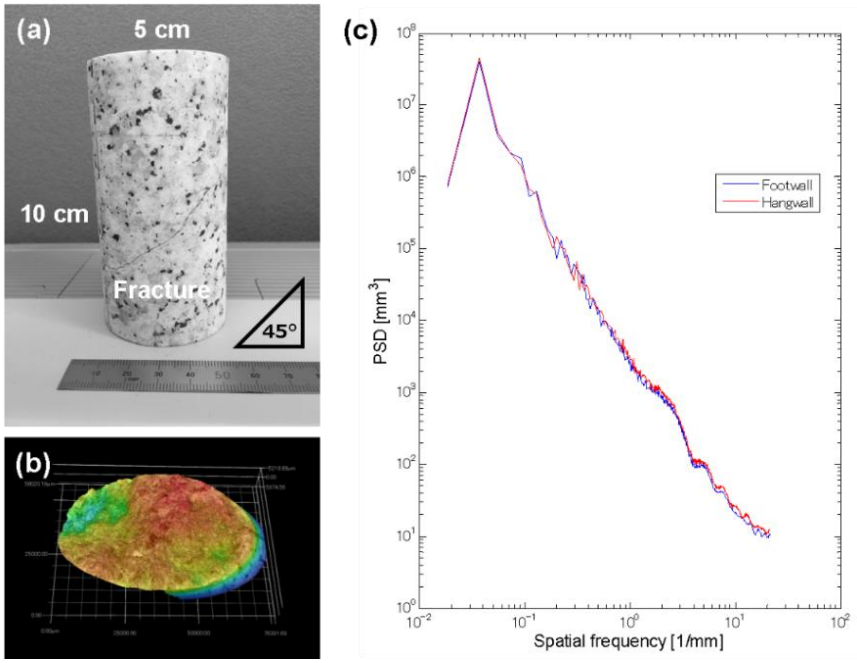

Figure 1: (a) Cylindrical sample of granite with a single tensile fracture, (b) Surface profiling of tensile fracture of granite, and (c) Relationship between power spectral density and spatial frequency for fracture surface roughness.

After fracture surface characterization, we set the cylindrical fractured sample in our experimental system for the shear-flow coupled experiment (Figure 2a), that is installed in Fukushima Renewable Energy Institute, AIST. The basic performance of the system is as following; maximum axial stress, confining stress, and pore pressures are 250 MPa, 40 MPa, and 70 MPa respectively, and the maximum temperature is 240℃. Silicone oil is used as the pressure medium for confining stress. Axial stress and axial displacement of the fractured sample are measured at both inside and outside of pressure vessel. In our experimental system, as confining stress, inlet fluid pressure, and outlet fluid pressure are independently controlled by three syringe pumps (i.e., Pump A, B, and C (Teledyne ISCO, 260D, 500D, and 500D)), we can evaluate the fracture permeability, storage volume within fracture, and so on accurately. The sampling frequency for the data logging is set to 100 Hz in the present study. In addition, we also monitor the Acoustic emissions (AEs) outside of the pressure vessel during the experiments. We use two AE sensors (R15a, Physical Acoustics) and DiSP system (Physical Acoustics), where preamplifier/threshold are set to 40/50 dB respectively and event counting method is adopted.

Ishibashi et al. (2018) have reported two types of hydraulic shear slip experiments (constant axial pressure control and constant axial displacement control) under relatively low stress states (e.g., normal stress on the fracture plane is between 52 and 58 MPa). As shear slip displacement is extremely large under the constant axial pressure control and it is not realistic that the crustal stress recovers immediately after the shear slip, we choose the constant axial displacement control in the present study. To determine the failure criteria, we first conducted the hydraulic shearing experiment under four different confining stress states (i.e., σ_{conf} = 8, 10, 18 and 24 MPa). In the experiments, we gradually increase the axial load to imitate the critically stressed state of fractures and the stress dependency of fracture permeability is evaluated within this procedure. Once the critically stressed state is achieved, we start injecting water via the borehole and increase pore pressure step by step to induce shear slip on the fracture. The outlet pressure keeps the constant value of 1 MPa (Pump C) and the shear slip is validated by both the reduction of axial load and the increase in the AE accumulated hits. In the fluid injection experiments, we evaluate the stress state at the onset of shear slip, shear slip distance caused by fluid injection, and permeability evolution during hydraulic shearing. In evaluating fracture permeability, we assume the matrix permeability of Inada granite is negligible (between 10^{-19} m^2 and 10^{-18} m^2) and fracture permeability can be calculated based on the cubic law;

$$k = \frac{e_h^2}{12} \qquad (1)$$

where k is the fracture permeability, and e_h is the hydraulic aperture. Using Darcy's law, these parameters are related as:

$$e_h = \left(-\frac{12\eta L Q}{W \Delta P} \right)^{1/3} \qquad (2)$$

where Q is the flow rate, ΔP is the differential pressure ((P_{in} + P_{out})/2) and η is the fluid viscosity (1.002×10^{-3} Pa·s at 20°C for distilled water). L and W are the flow path length and the flow path width, which are in the parallel and perpendicular directions to the macroscopic fluid flow direction. L and W are set to 50.5 mm and 34 mm respectively by considering the geometry of the cylindrical core sample used in our study. While the fluid flows radially from the inlet borehole to outlet borehole, we assume the uniform planar flow within the fracture in this study. Note this discrepancy will not be a serious problem in estimating the hydraulic property of fractures.

With respect to the acoustic emissions, we evaluate the AE parameters for the respective AE hit (Figure 2b). Although the AE sensors are set outside of the pressure vessel, detected waveforms are not so noisy (Figure 2c), and we possibly evaluate these parameters. Based on these parameters, rise angle (defined as the rise time divided by maximum amplitude) and average frequency (defined as AE counts divided by duration time), which were introduced by Ohno and Ohtsu (2010) to classify tensile (Mode I) and shear (Mode II) fracture, are calculated. By tracking the time dependent change for the combination of these parameters, we discuss the failure processes during hydraulic shearing.

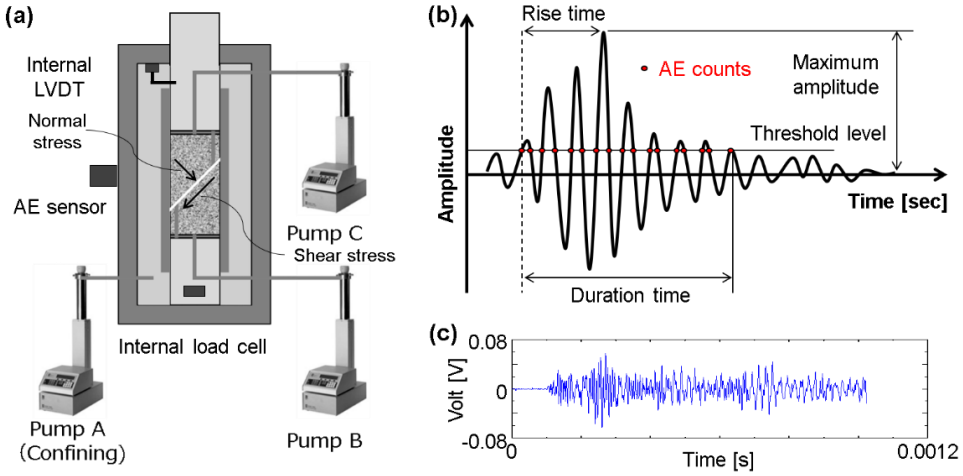

Figure 2: (a) Experimental configuration for measuring the fracture permeability and stresses working on the fracture plane during shearing, (b) AE parameters in an AE hit (modified from *Ohno and Ohtsu*, 2010), and (c) Representative AE waveform recorded during the pressurized water injection.

3. EXPERIMENTAL RESULTS

Figure 3a shows the relationship between the shear stress and effective normal stress before (open symbol) and at the onset (solid symbol) of fracture shearing. The differences between these two points at the same shear stress level corresponding to the pore pressure increases, ΔP_{pore}, which are required to trigger shear slip on the fracture. Note that ΔP_{pore} is consistently smaller than the confining stress, σ_{conf}, which corresponds to the minimum principal stress. Failure criteria on the hydraulic shearing for the rough surface fractures can be represented as;

$$\tau = 7.8 + 0.85(\sigma_n - P_{pore}) \qquad (3)$$

where τ is the shear stress, σ_n is the normal stress, and P_{pore} is the pore fluid pressure. Equation (3) suggests that the cohesive strength (C_0) is 7.8 MPa and frictional coefficient (μ) is 0.85. Figure 3b shows the relationship between the fracture permeability and the effective normal stress of the rock fractures. Fracture permeability decreases with increasing effective normal stress and absolute permeability values are comparable with those in previous studies (Ishibashi et al., 2015; Ye and Ghassemi, 2018). These permeabilities (from 3×10^{-13} m^2 to 3×10^{-12} m^2) are the standard values and we evaluate how much fracture permeability increases with respect to these reference values. Figure 3c shows the relationship between the shear slip displacement and shear stress. Except for one point at the shear stress of 60 MPa, shear slip displacement generally increases with increasing the shear stress. As the permeability increase is closely related to the fracture opening, which can be approximated as a product of the shear slip displacement and the dilation angle, such a stress dependency of shear slip displacement is essential to optimize EGS design.

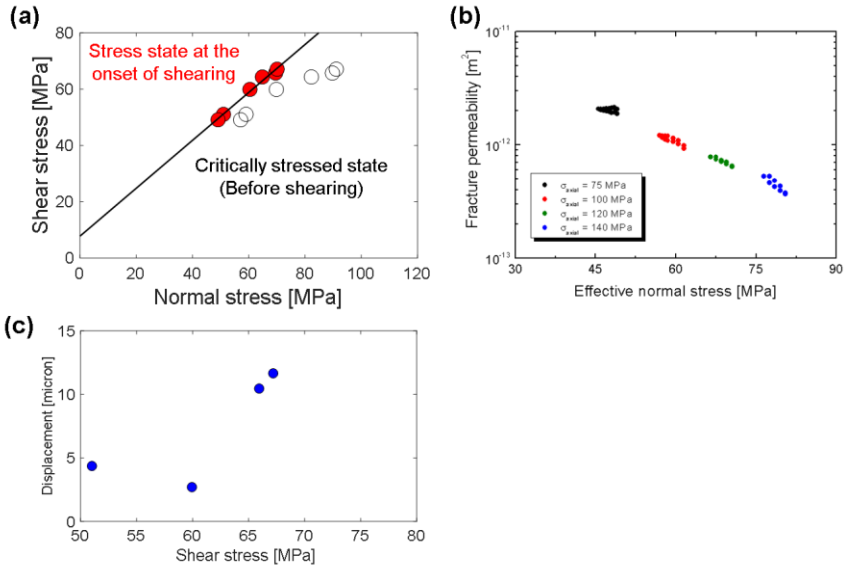

Figure 3: (a) Relationship between shear stress and normal stress before and at the onset of fracture shearing, (b) relationship between fracture permeability and effective normal stress before shea slip and (c) dependence of shear slip displacement on the shear stress working on the fracture.

Dynamic behaviours in mechanical and hydraulic properties during hydraulic shearing are shown in Figure 4, where we focus on the section at the onset of shear slip triggered by the pressurized water injection. Figure 4 corresponds to the results at a confining pressure of 24 MPa. We can find that the shear slip occurs at ~11,668 seconds after the start of the experiment. The occurrence of shear slip is supported by changes both in axial stress (Figure 4a) and axials displacement (Figure 4b). The order of shear slip velocity is roughly calculated to be 10^{-6} m/sec and is well comparable to that reported in the meso-scale fault reactivation experiment (Guglielmi et al., 2015a and 2015b). On the other hands, prior to the shear slip, we can observe that fracture permeability starts increasing (Figure 4c) and the AE accumulated hits also start increasing (Figure 4d). Initial fracture permeability is 1.2×10^{-12} m^2 in this experiment, and this value is increased to be 5.8×10^{-12} m^2 at maximum (around 5 times). Such a permeability increase may be explained via the self-propping mechanism caused by the surface roughness of rock fracture s (Esaki et al., 1999; Ishibashi et al., 2016; Ye and Ghassemi, 2018), but we need to carefully explore how much permeability enhancement can be maintained after pore fluid depressurization.

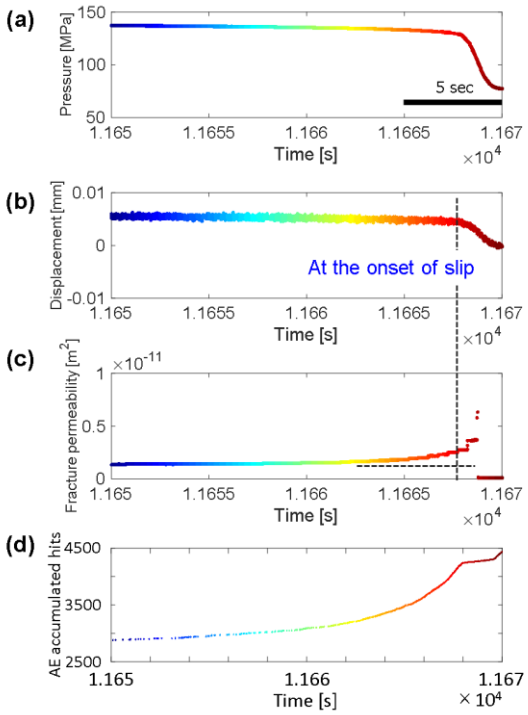

Figure 4: Time dependent changes of (a) axial stress measured by the internal load cell, (b) axial displacement measured by the internal LVDT, (c) fracture permeability, and (d) AE accumulated hits detected outside of the pressure vessel. These correspond to the results at a confining pressure of 24 MPa.

Figure 5a shows the time dependent change for the combination of average frequency and rise angles. Grey shaded area in Figure 5a corresponds to the boundary of tensile fracture and shear fracture. Note that the location of the boundary can't be specified, and the statistical processing is required for their classification in future. As such, although there are uncertainties in data interpretation, we can quantitatively track time dependent change in the failure process during hydraulic shearing. Before the onset of fracture shearing (~11,668 sec), most of the AE events are classified in the left side of Figure 5a (i.e., tensile fractures). This observation suggests that stress concentrations are formed around the contacting asperities prior to the shear slip, that leads to the occurrence of tensile fractures, weakening fracture asperities, and associated porosity/permeability enhancement of fracture. In contrast, after the onset of fracture shearing, the AE events of both tensile and shear modes are distributed in Figure 5a. This result suggests that not only shear slip but also fracture propagation should be taken into consideration when the hydraulic shearing of "rough surface's fracture" is simulated. The importance of such a "mixed mode" concept is recognized in interpreting the field observations at the actual EGS test site (Norbeck et al., 2018). In addition, Figure 5b shows the X-ray CT image of rock sample captured after the experiment (Scan Xmate D225RSS270, Comscantecno), and we can find the development of new fractures at the middle of the pre-existing fractures. This result strongly suppors the concept of "mixed mode" fracturing. As the newly created fractures potentially help to improve the fracture connectvity and associated bulk permeability in the reservoir scales, the detail of hydraulic shear process/senario should be further explored to fix the constitutive model equations.

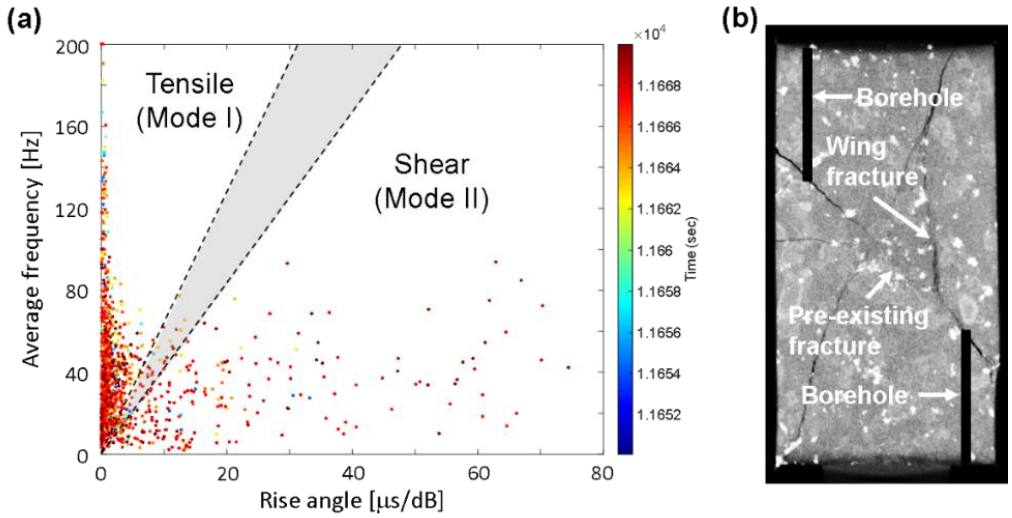

Figure 5: (a) Relationship between average frequency and rise angle for the respective AEs detected during fracture slip and (b) X-ray CT image of rock sample after the experiment. We can find the development of wing fracture from the middle of the pre-existing fracture.

4. DISCUSSION AND CONCLUSION

We explore the dynamic behaviours in mechanical and hydraulic properties of granite fracture during hydraulic shearing at the imitate condition of the geothermal reservoirs. Experimental results identify that: (1) Coulomb criteria is applicable to predict the onset of hydraulic shearing, (2) shear slip displacement generally increases with increasing the shear stress, (3) permeability increase due to the self-propping mechanism of rough surface's fracture, (4) not only shear slip but also fracture propagation occur when the rough surface's fracture are hydraulically sheared (i.e., mixed mode concept).

Based on the experimental results, shear slip displacement (δ), which closely links to the permeability change (Ishibashi et al., 2016), is estimated as a function of the length associated with the pressurized zone, r (Fig. 6) under the quasi-geothermal reservoir environments. In our experiments, r is equivalent to the distance between two boreholes (50.5 mm). Based on the present experimental results, the ratio of δ to r is 4.4×10^{-5} (0.0044%) in stress relaxation state under low stress, whereas δ/r is 1.9×10^{-4} (0.019%) in stress relaxation state under high stress. These relationships are shown in Fig. 6 and constrain the maximum and the minimum bounds of hydraulically triggered shear slip. Estimated values of slip distance for the re-activation experiments of mesoscale faults (Guglielmi et al., 2015a and 2015b) are also plotted in Fig. 6 for comparing the shear displacements between in laboratory-scale and in mesoscale. Despite the stress state and the rock type are different between laboratory- and mesoscale-experiments, we find that the shear displacements of the mesoscale fractures are within the range of our suggested empirical formulas. Since the δ-r relationships are influenced by many factors such as surface roughness, shear modulus, strength, friction, and so on, further studies are essential. In particular, as the mechanical parameter values of granite decrease significantly with increasing temperature, slopes constraining the δ-r relation in Fig. 6 may be decreased in actual geothermal reservoir environments (>300°C). Again, as the amount of shear slip undoubtedly constrains the permeability increase (Ishibashi et al., 2016), it is considered that the present study possibly links to how much the fracture permeability can be increased due to shear slip under the geothermal reservoir environment.

In summary, our results are fundamental in designing the permeable zone within deep geothermal reservoirs and for reducing the risk of triggered earthquakes during pressurized water injection into the reservoirs. Moreover, such information would be indispensable to determine the actual injection protocol in the EGS developments.

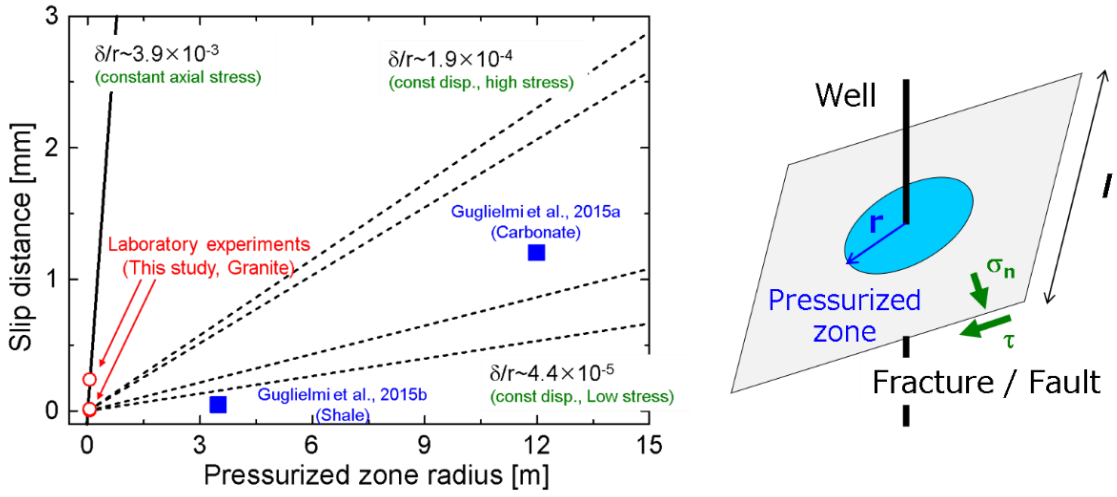

Figure 6: Comparison of the shear/slip displacement -pressurized zone radius relations between the laboratory experiments and the field (mesoscale) experiments (Guglielmi et al., 2015a; Guglielmi et al., 2015b)

ACKNOWLEDGEMENTS

The present study was supported in part by METI, Japan through the International Research Program for Innovative Energy Technology. This support is gratefully acknowledged.

REFERENCES

Ellsworth, W. L., Injection-Induced Earthquakes, *Science*, **341**, (2013), 142-149

Esaki, T., S. Du, Y. Mitani, K. Ikusada, and L. Jing, Development of a shear-flow test apparatus and deformation of coupled properties for a single rock joint, *Int. J. Rock Mech. Min. Sci.*, **36**, (1999), 641-650

Evans, F. E., A. Genter, J. Sausse, Permeability creation and damage due to massive fluid injections into granite at 3.5 km at Soultz; 1. Borehole observations, *J. Geophys. Res.*, **110**, (2005), B04203

Guglielmi, Y., F. Cappa, J. P. Avouac, P. Henry, and D. Elsworth, Seismicity triggered by fluid injection-induced aseismic slip, *Science*, **348**, (2015a), 1224-1226

Guglielmi, Y., D. Elsworth, F. Cappa, P. Henry, C. Gout, P. Dick, and J. Durand, In situ observations on the coupling between hydraulic diffusivity and displacements during fault reactivation in shales, *J. Geophys. Res.*, **114**, (2015b), 1-15

Häring, M.O., U. Schanz, F. Ladner, and B.C. Dyer, Characterization of the Basel 1 enhanced geothermal system, *Geothermics*, **37**, (2008), 469–495

Ishibashi, T., N. Watanabe, H. Asanuma, and N. Tsuchiya, Linking microearthquakes to fracture permeability change: The role of surface roughness, *Geophys. Res. Lett*, **43**, (2016), 7486-7493

Ishibashi, T., H. Asanuma, S. Ishikawa, and N. Watanabe, Concurrent monitoring of hydraulic and mechanical properties of granite fracture during hydraulically induced shearing in laboraoty, *52nd US Rock Mechanics/Geomechanics Symposium*, (2018), ARMA-2018-369

Ikari, M. J., A. R. Niemeijer, and C. Marone, The role of fault zone fabric and lithification state on frictional strength, constitutive behaviour, and deformation microstructure, *J. Geophys. Res. Solid Earth*, **116**, (2011), B08404

Kohli, A. H. and M. D. Zoback, Frictional properties of shale reservoir rocks, *J. Geophys. Res. Solid Earth*, **118**, (2013), 5109-5125

Majer, E. L., R. Baria, M. Stark, S. Oates, J. Bommer, B. Smith, and H. Asanuma, Induced seismicity associated with Enhanced Geothermal Systems, *Geothermics*, **36**, (2007), 185–222

Norbeck, J. H., M. W. McClure, and R. N. Horne, Field observations at the Fenton Hill enhanced geothermal system test site support mixed-mechanism stimulation, *Geothermics*, **74**, (2018), 135-149

Ohno, K., and M. Ohtsu, Crack classification in concrete based on acoustic emission, *Constr. Build. Mater.*, **24**, (2010), 2339-2346

Rutter, E. and A. Hackston, On the effective stress law for rock-on-rock frictional sliding, and fault slip triggered by means of fluid injection, *Phil. Trans. R. Soc.* A., **375**, (2017), 20160001

Ye, Z., and A. Ghassemi, Injection-induced shear slip and permeability enhancement in granite fractures, *J. Geophys. Res. Solid Earth*, **123**, (2018), 9009-9032